www.nature.com/aps

Acta Pharmacologica Sinica

ARTICLE

Gossypol, a novel modulator of VCP, induces autophagic degradation of mutant huntingtin by promoting the formation of VCP/p97-LC3-mHTT complex

Xiao-jing Li[1], Yuan-yuan Zhang[2], Yu-hua Fu[3], Hao Zhang[2], He-xuan Li[3], Quan-fu Li[1], Hai-ling Li[1], Ren-ke Tan[1], Chen-xiao Jiang[1], Wei Jiang[1], Zeng-xia Li[1], Cheng Luo[2], Bo-xun Lu[3] and Yong-jun Dang[1]

Huntington's disease (HD) is an autosomal dominant neurodegenerative disorder caused by toxic aggregates of mutant huntingtin protein (mHTT) in the brain. Decreasing mHTT is a potential strategy for therapeutic purpose of HD. Valosin-containing protein (VCP/p97) is a crucial regulator of proteostasis, which regulates the degradation of damaged protein through proteasome and autophagy pathway. Since VCP has been implicated in pathogenesis of HD as well as other neurodegenerative diseases, small molecules that specifically regulate the activity of VCP may be of therapeutic benefits for HD patients. In this study we established a high-throughput screening biochemical assay for VCP ATPase activity measurement and identified gossypol, a clinical approved drug in China, as a novel modulator of VCP. Gossypol acetate dose-dependently inhibited the enzymatic activity of VCP in vitro with IC_{50} of 6.53±0.6 μM. We further demonstrated that gossypol directly bound to the interface between the N and D1 domains of VCP. Gossypol acetate treatment not only lowered mHTT levels and rescued HD-relevant phenotypes in HD patient iPS-derived Q47 striatal neurons and HD knock-in mouse striatal cells, but also improved motor function deficits in both *Drosophila* and mouse HD models. Taken together, gossypol acetate acted through a gain-of-function way to induce the formation of VCP-LC3-mHTT ternary complex, triggering autophagic degradation of mHTT. This study reveals a new strategy for treatment of HD and raises the possibility that an existing drug can be repurposed as a new treatment of neurodegenerative diseases.

Keywords: Huntington disease; mutant huntingtin protein; gossypol acetate; VCP; LC3; autophagic degradation; drug reposition

Acta Pharmacologica Sinica (2021) 42:1556–1566; https://doi.org/10.1038/s41401-020-00605-0

INTRODUCTION

Neurodegenerative disorders include many diseases caused by progressive loss of neurons. A hallmark of most neurodegenerative diseases is aberrant accumulation and aggregation of misfolded proteins inside neurons, including mutant huntingtin (mHTT) aggregates in Huntington's disease (HD) [1], mutant ataxin-3 in spinocerebellar ataxia type 3/Machado–Joseph disease (SCA3/MJD) [2], amyloid-beta (Aβ or amyloid-beta) in Alzheimer's disease (which also has extracellular aggregates) [3], and α-synuclein in Parkinson's disease [4]. HD is an appealing model for pathological study and for drug discovery for degenerative diseases because of its simple genetics and its relatively high prevalence [5]. It is an autosomal dominant neurodegenerative disorder caused by toxic aggregates of mutant HTT proteins (mHTT) in the brain [6]. HTT exon 1 contains a polyglutamine (polyQ) tract that consists of 6–35 glutamine residues in normal neurons. Mutant HTT proteins with expansions with more than 35 glutamine residues induce protein misfolding and are more prone to aggregation, leading to the onset of HD. The ability of neurons to target these aggregates for degradation is insufficient, causing protein accumulation, aggregation, and protein dyshomeostasis, a common manifestation in neurodegenerative diseases [7]. mHTT abundance and proteostasis are indicators of neurodegeneration and disease severity [8]. Thus, induction of the degradation of disease-causing proteins is expected to prevent aggregate accumulation and neuronal cell death, representing a general therapeutic strategy for HD and other neurodegenerative disorders.

Valosin-containing protein (VCP/p97) is a central and important regulator of proteostasis and has been implicated in degenerative diseases [9]. Chaperone VCP protein (p97 in mouse, TER94 in *Drosophila melanogaster*, and CDC48 in *S. cerevisiae*) belongs to the AAA protein family of ATPases [10]. VCP is composed of an N-terminal domain, followed by tandem D1 and D2 ATPase domains joined by a linker region. VCP forms a hexametric ring with a cylindrical structure and the N-terminal domain that allows VCP to interact with adapter or substrate proteins. VCP regulates the degradation of damaged proteins and organelles through the proteasome and autophagic pathways [11–13] and has been linked both directly and indirectly to

[1]Key Laboratory of Metabolism and Molecular Medicine, the Ministry of Education, Department of Biochemistry and Molecular Biology, School of Basic Medical Sciences, Fudan University, Shanghai 200032, China; [2]Drug Discovery and Design Center, The Center for Chemical Biology, State Key Laboratory of Drug Research, Shanghai Institute of Materia Medica, Chinese Academy of Sciences, Shanghai 201203, China and [3]Neurology Department at Huashan Hospital, State Key Laboratory of Medical Neurobiology, School of Life Sciences, Fudan University, Shanghai 200438, China
Correspondence: Cheng Luo (cluo@simm.ac.cn) or Bo-xun Lu (luboxun@fudan.edu.cn) or Yong-jun Dang (yongjundang@fudan.edu.cn)
These authors contributed equally: Xiao-jing Li, Yuan-yuan Zhang, Yu-hua Fu

Received: 22 July 2020 Accepted: 23 December 2020
Published online: 25 January 2021

neurodegenerative disorders. In HD and other polyQ-related diseases, endogenous VCP colocalizes with polyQ-containing aggregates in cultured polyQ-expressing neuronal cells [14]. Colocalization of VCP with disease-causing aggregates has been reported in not only Huntington disease but also in Machado–Joseph disease (MJD) and Parkinson's disease [15, 16]. Furthermore, missense mutations in the VCP gene have been implicated in the pathogenesis of human degenerative disorders, including IBMPFD (inclusion body myopathy associated with Paget disease of bone and frontotemporal dementia) and rare cases of familial amyotrophic lateral sclerosis (ALS) [9]. These results have emphasized the importance of VCP in the pathology of human neurodegenerative disorders and raised the possibility of targeting VCP to treat HD and other neurodegenerative disorders.

One of the crucial mechanisms for clearing the disease-causing mHTT protein in HD is through macroautophagy (hereafter autophagy). Autophagy is a highly conserved cellular process in which cytosolic components, including damaged organelles, misfolded proteins, and aggregates, are engulfed for degradation, to maintain cytosolic homeostasis [17]. It mediates the degradation of large disease-related proteins or aggregates that cause neurodegenerative diseases and are mostly inaccessible to the proteasome [18]. In HD, the abnormal accumulation of mHTT proteins is by insufficient autophagy machinery [19]. Strategies that induce moderate autophagy upregulation are believed to be of therapeutic benefit for patients with HD or other neurodegenerative diseases [20, 21]. Microtubule-associated protein 1A/1B-light chain 3 (LC3), the core autophagy component in mammalian cells, plays a pivotal role in the autophagy-lysosome pathway, regulating both autophagosome formation and cargo recognition [22]. LC3 has been demonstrated to recognize protein aggregates for autophagy removal [23]. It has been reported that LC3 colocalizes with mHTT aggregates and facilitates mHTT protein degradation by autophagy [24, 25]. VCP can interact with LC3 [26] and has also been reported to colocalize with mHTT [14], indicating the potential involvement of VCP in autophagy-mediated mHTT degradation. However, the role of VCP in autophagy-mediated mHTT clearance remains unclear.

To explore the potential treatment of HD by small molecules targeting VCP, we established a high-throughput screening (HTS) assay using VCP ATPase activity as a readout and identified gossypol acetate (GA) as a novel modulator of VCP. GA acts in a gain-of-function inducer of mHTT-VCP-LC3 complex formation, enabling autophagy-mediated degradation of endogenous mHTT. GA reduced mHTT levels, alleviated toxicity in HD neurons and ameliorated disease-related behaviors in *Drosophila* and mouse HD models, making GA a promising lead compound for the development of new HD therapies.

MATERIALS AND METHODS

High-throughput screening

A malachite green-based ATPase assay was used to screen the natural compound library in our laboratory. The assay procedure was adopted from previous reports with the modifications described herein [27]. Colorimetric determination of VCP ATPase activity was performed as follows: 1 μM 6×His-VCP or the corresponding fragments were incubated with reaction buffer containing 100 mM Tris-HCl (pH 7.5), 6 mM $MgCl_2$, 20 mM KCl, and 0.01% Triton X-100. An aliquot (15 μL) of this mixture and the tested compound (40 μM) was added into each well of a 96-well plate. After incubation for 1 h at 4 °C, 10 μL of ATP was added into each well to start the reactions. After incubation of the reaction mixture for 30 min at 37 °C, an aliquot of 80 μL of malachite green reagent was added to each well, and 10 μL of 34% sodium citrate was immediately used to stop the hydrolysis of ATP. The samples were mixed thoroughly and incubated at 37 °C for another 15 min. The absorbance of each well at OD_{620} was then measured by a FlexStation3 (Molecular Devices, SJ, CA, USA). Enzymatic activity is calculated by curve fitting (based on the Michaelis–Menten model) using GraphPad Prism 5 software.

Plasmid construction, protein expression, and purification

Human wild-type VCP protein (residues 1–806) and VCP fragment proteins, including the N domain (residues 1–188), N-D1 domain (residues 1–481), D2 domain (residues 461–806), and D1-D2 domain (residues 188–806), were subcloned into a pET-28a(+) vector, and the proteins were expressed in *E. coli* BL21 (DE3) with His-tags. GST and GST-LC3B were expressed in *E. coli* BL21 (DE3) with GST tags.

For the expression of recombinant His-tagged proteins, *E. coli* BL21 (DE3) containing the desired plasmid was grown in LB medium containing 50 μg/L kanamycin with shaking at 37 °C to an OD_{600} of 0.5–1. Then, the cell culture was cooled to 18 °C, induced with 1 mM IPTG and harvested 16 h later by centrifugation. The cells were lysed with lysis buffer (150 mM NaCl, 1% Triton X-100, 50 mM Tris-HCl (pH 8.0), 20 mM imidazole, 5% glycerol, 5 mM $MgCl_2$, 2 mM β-mercaptoethanol, 0.1% lysozyme, and a protease inhibitor (PMSF). The lysate was centrifuged at 10,000 rpm for 30 min at 4 °C, and the supernatant was loaded onto Ni-NTA resin (QIAGEN, 30210, DUS, DE) at 4 °C with rotation for 60 min and washed with a buffer containing 150 mM NaCl, 50 mM Tris-HCl (pH 8.0), 20 mM imidazole, 5% glycerol, and 5 mM $MgCl_2$. The recombinant proteins were eluted with a 50–250 mM imidazole gradient, concentrated by Centriprep (Millipore, UFC901096, MA, USA), and maintained in storage buffer (150 mM KCl, 50 mM Tris-HCl (pH 7.5), 1 mM $MgCl_2$, 20% glycerol).

Recombinant GST-fused proteins were expressed in *E. coli*, purified with glutathione-Sepharose, and eluted with 25 mM glutathione, and the buffers were exchanged into 150 mM KCl, 50 mM Tris-HCl (pH 7.5), 1 mM $MgCl_2$, and 20% glycerol with a desalination column. Protein concentrations were determined by a Pierce® BCA protein assay kit (Thermo, 23225, SHH, CN), and protein purity was determined by SDS-PAGE and Coomassie blue staining.

Partially proteolysis assay

Trypsin digestion was performed in storage buffer (50 mM Tris-HCl, pH 7.0; 150 mM NaCl; 10% glycerol; 1 mM DTT; and 1 mM EDTA). VCP (10 μM), and the compounds (15 μM, final DMSO concentration of 1%) were incubated for 1 h at 37 °C in a total volume of 50 μL. DMSO (1 μL) was a control. The reaction was started by the addition of trypsin, and then, samples were incubated at 37 °C. The reaction was immediately stopped by the addition of 10 μL of 6× sample buffer heated at 100 °C for 10 min. The digestion products were separated on 10% SDS-PAGE gels, and the bands were visualized by Coomassie blue staining.

Protein thermal shift assay

A protein thermal shift (PTS) assay was used to assess the thermal stability change of purified VCP and VCP fragment proteins in the presence of GA. Three micrograms of 6×His-VCP full-length protein or 6×His-VCP fragment protein were incubated with 5 μM GA on ice for 30 min (100 mM Tris-HCl, pH 7.5, and 150 mM NaCl), and then subjected to a temperature gradient (50, 56.8, 64.3, 72.0, 64.3, and 72.0 °C) using the T100 Thermal Cycler PCR instrument. After heating, the samples were centrifuged at 12,000 r/min for 2 min at 4 °C. The supernatant was transferred and stored for use in detecting retained soluble protein by Coomassie blue staining. The intensity of the bands was obtained by grayscale scanning with ImageJ, and the T_m value was calculated by Boltzmann fitting using GraphPad Prism 5 software.

Isothermal titration calorimetry

Isothermal titration calorimetry (ITC) measurements were carried out at 25 °C on a Nano ITC calorimeter. Proteins were extensively dialyzed against 20 mM sodium phosphate, pH 7.0; 200 mM KCl; and 5 mM β-mercaptoethanol (β-ME) and degassed for 15 min

before each experiment. Full-length VCP was placed in the syringe and titrated as ligands into a sample cell containing VCP. The first technical injection of 0.4 μL was followed by 25 injections of 2 μL into the sample cell (300 μL) using 250-rpm stirring and a 200-s delay between successive injections. At least three titration experiments were performed for each ligand, and the data were corrected for the heat generated by the dilution by injecting the same ligand concentration into an identical buffer. The corrected data were analyzed with a one-site binding model and nonlinear least-squares fitting to derive the K_D value using the NanoAnalyze 3.5.0 software package.

Pull-down experiments

Recombinant VCP (residues 1–806) and N-D1 (residues 1–481) and D2 (residues 461–806) were incubated with GA (5, 10, and 15 μM) for 2 h at 4 °C in 0.6-mL buffer (50 mM Tris-HCl, pH 7.5; 150 mM NaCl; and 0.2% Triton-X-100) followed by the addition of GST/GST-LC3/Htt-Q25/Htt-Q72 for 2 h. Then, the cells were incubated with GST beads for 1 h. The immunoprecipitates were washed four times with 1× PBS and 0.2% Triton-X-100 buffer and analyzed by SDS-PAGE and Western blot analysis.

Cell culture and transfection

Human HEK293T cells were purchased from ATCC. STHdh cells (CH00096 – Q111/Q7) were obtained from Coriell Cell Repositories. Patient-derived Q47 iPS-derived striatal neurons were obtained from a Mongolian Huntington's disease patient. The generation and authentication of the Huntington's Disease origin of the iPS-derived neurons were described previously [28]. The study was approved by The Ethics Community of Institutes of Biomedical Sciences at Fudan University.

Human HEK293T cells and mouse STHdh cells were cultured in DMEM (Gibco, 11965092, SHH, CN) supplemented with 10% (*v*/*v*) fetal bovine serum (FBS) and antibiotics (penicillin and streptomycin). iPSCs were cultured in Essential 8 medium (Gibco, A1517001, SHH, CN), and the Q47 iPS-derived striatal neurons cells were grown and maintained in neuron medium (Neural Basal + N2 + B27 + BDNF + GDNF + IGF + Vitamin C and antibiotics). All mammalian cell lines were maintained in a 37 °C incubator with 5% CO_2, except the STHdh cells, which were maintained at 33 °C with 5% CO_2.

Cells were plated at a density of 30% and split whenever they reached 90% confluence. Before transfection, the cells were seeded in 10-cm dishes and reached 70% confluence the next day. For transfection, 10 μg of plasmid DNA and 30 μL of PEI (polyethylenimine) were added to 500 μL of MEM (Gibco, 12571071, SHH, CN). The reaction mixture was mixed by pipette. After incubation for 30 min at RT, the solution was added dropwise to the cells.

The protocol for neuron siRNA transfection was described previously [29]. The siRNAs were reverse transfected into iPS-derived neurons with Lipofectamine RNAiMAX (Life Technologies, 13778, SHH, CN). All transfections were performed according to the manufacturer's protocol. The cells were harvested 3 days after siRNA transfection or 2 days after cDNA transfection for Western blot, Homogeneous time-resolved fluorescence (HTRF) or immunofluorescence analyses of neuronal loss and apoptosis. The following siRNA target sequences were used (with the supplier information):

Scrambled (nontargeting) siRNA: siRNA: 5′-UUCUCCGAACGU GUCACGUTT-3′ (Invitrogen, D-001810-10, SHH, CN);

HTT siRNA: targeting 5′-CAGGUUUAUGAACUGACGUUA-3′.

Homogeneous time-resolved fluorescence assay

The HTRF assays were performed similar to those previously described [30]. The antibody pair concentrations were 0.023/1.4 μg/mL (in HTRF buffer with 1% Triton X-100) and were optimized for different antibody pairs and cell lines in different experiments. For the human fibroblasts and human iPS-derived neurons, the antibody pair was 2B7/MW1. For the mouse STHdh cells and mouse brain tissue, the antibody pair was 2B7/2166. For all the experiments, the protein concentration (by BCA, Pierce, 23225, SHH, CN) was measured to ensure equal loading or cell viability. Different protein concentrations or number of cells per well were tested to ensure that the signals were in the linear range. Background corrections were performed by subtracting the background signals obtained from blank samples.

Neuronal loss and apoptosis measurements

The iPS-derived neurons obtained from patients exhibited HD-dependent phenotypes, including elevated caspase-3 signaling and neuronal loss upon BDNF elimination. Fluorescent dye was used to measure the apoptosis phenotype, and immunostaining of Tuj1, a neuronal-specific tubulin that captures neuronal morphology, was used to measure the neuronal shrinkage and phenotype loss. STHdh cells exhibit HD-dependent caspase-3 activity upon stress, such as that caused by serum removal. For use in these cells, the compounds were diluted in DMSO and added to the cells at least 1 day after plating (for iPS-derived neurons, the compounds were added one week after plating). The cells were stressed (BDNF was removed from the iPS-derived neurons) 1 day after compound treatment and tested at the indicated time points. For caspase-3 activity detection, NucView 488 caspase-3 dye (Biotium, 30029, CA, USA) was used as an indicator of apoptosis. To assay neuronal loss, Tuj1, a neuronal-specific tubulin, was stained to show neuronal morphology. Images were taken by Carl Zeiss microscopes and analyzed blindly by ImageJ for caspase-3 and Tuj1 quantification (Covance, MMS-435P, NJ, USA).

Western blot analysis

HeLa cells were plated at 75% confluence in 24-well plates. Sixteen hours after plating, the cells were treated with the tested compounds at the indicated concentrations for 24 h. Then, the cells were lysed on ice in 6× SDS sample buffer (62.5 mM Tris-HCl, pH 6.8; 5% β-mercaptoethanol; 10% glycerol; and 0.01% bromophenol blue) for 30 min in the presence of protease inhibitors (Roche Diagnostics, SHH, CN). Proteins were resolved by SDS-PAGE and transferred onto an NC membrane (Millipore, MA, USA) for semidry Western blotting. The membrane was blocked with 5% milk in PBST (1× PBS, 0.5% Tween 20) and incubated overnight with the indicated primary antibody in 5% BSA in PBST at 4 °C. The membrane was then washed three times using PBST and incubated with the HRP-conjugated secondary antibody (Jackson ImmunoResearch, 115-035-003, PA, USA) diluted 1:10,000 in 5% BSA with PBST for 1 h at RT, washed again three times (5 min each time) with PBST, and incubated with ECL reagent mixture (Thermo, A38555, SHH, CN). Chemiluminescence signals were detected using a ChemiScope 3400 Mini (Shanghai Clinx Inc, SHH, CN).

Autophagic flux assay

For confocal microscopy studies of autophagic flux, mCherry-EGFP-LC3 stable HeLa cells were plated at 50%–65% confluency on glass coverslips. Sixteen hours after plating, the cells were treated with the indicated molecules (GA, rapamycin, and CQ) for 24 h. Stable mCherry-GFP-LC3-expressing HeLa cells were fixed and permeabilized in cold methanol for 10 min at 4 °C. After three PBS washes, the cells were fixed on slides using immunostained sealant with DAPI (Vector Laboratories, H-1200, Burlingame, CA, USA). Confocal images were acquired using a Leica LSM510 NLO system with Argon 488 nm, 543 nm HeNe, and a Coherent Chameleon XR 2p laser with appropriate excitation and emission filters.

In vivo *Drosophila* model

The elav-GAL4 nervous system-driver cell line and the UAS-fl-HTT-Q128 cell line (expressing human full-length HTT with 128Q when crossed to the GAL4 line) were obtained from the Bloomington *Drosophila* Stock Center at the University of Indiana (http://flystocks.bio.indiana.edu/). The UAS-HTT-exon1-Q72 cell line was generated by injecting the pUAST-HTT-exon1-Q72 vector into w1118 *Drosophila* embryos, and the UAS-HTT-exon1-Q72 was integrated into chromosome 2 [31]. This cell line expressed the human HTT-exon1 N-terminal fragment with 72Q when crossed with the GAL4 cell line, and the expression was validated by both HTRF (see the "GA reduced the mHTT protein level and neuronal toxicity section" section) and Western blot analysis.

For the *Drosophila* behavioral experiments, we placed 15 age-matched virgin female flies in an empty vial and tapped them down. The percentage of flies that climbed past a 9-cm-high line after 10 s was recorded and analyzed by two-way ANOVA tests. For the survival analysis, we recorded the survival of 15 age-matched virgin female flies during feeding with GA. The survival time of the flies was recorded and analyzed by two-way ANOVAs.

Mouse behavioral experiments

The generation and characterization of Hdh140Q knock-in mice have been previously described [29]. All behavioral experiments were performed during the light phase, and the experimenters were blinded to the genotype of each mouse. Both males and females were used. All the mice were kept in a behavioral test room in dim red light for one hour before the start of the experiments. For the activity tests, mice were placed in a pen holder with a mashed surface (98 mm height × 91 mm diameter) for 5 min. The number of times the mouse rears indicates the total number of events when the animal was on two (or one) hindlimbs. For open-field tests, mice were placed in a 30 cm × 30 cm × 40 cm white Plexiglas chamber (Med Associates, GA, USA) in a behavior room, and locomotion was captured by camera on top of the chamber and recorded for 15 min. The traveling trace and distance were then analyzed with the Med-Associates Activity Monitor program.

Study approval

The mouse experiments were carried out following the general guidelines published by the Association for Assessment and Accreditation of Laboratory Animal Care. The protocol used in animal experiments was approved by the Animal Care and Use Committee of the School of Medicine at Fudan University (Approval #20140904).

Statistical analysis

Biochemical experiments were repeated at least three times. Values are reported as the means ± SD (GraphPad Prism 5, San Diego, CA, USA). Statistical comparisons between two groups were analyzed using unpaired two-tailed *t*-test. Statistical comparisons among multiple groups were conducted using one-way ANOVA (GraphPad Prism 5, San Diego, CA, USA). Statistical comparisons for a series of data collected at different time points were conducted by ANOVA. All statistical tests were unpaired and two-tailed.

Materials

The antibodies used in this study were anti-GFP (Proteintech, 66002-1-Ig, Rosemont, IL, USA), anti-LC3 (Novus, NB100-2220, SHH, CN), anti-P62 (Proteintech, 66184-1-Ig, Rosemont, IL, USA), anti-NCOA4 (Santa Cruz, sc-373739, Dallas, TX, USA), anti-NDP52 (Novus, NBP2-19499, USA), anti-NBR1 (Santa Cruz, sc-130380, Dallas, TX, USA), anti-GAPDH (Proteintech, 60004-1-Ig, Rosemont, IL, USA), anti-ub (Proteintech, Rosemont, 10201-2-AP, IL, USA), anti-VCP (Proteintech, 60316-1-Ig, Rosemont, IL, USA), anti-β-tubulin (Proteintech, 10094-1-AP, Rosemont, IL, USA), and anti-Flag (Novus, NBP1-06712, SHH, CN). The HTT antibody 2B7 and the polyQ antibody MW1 [29] have been described previously. The probes used for Western blotting were anti-mouse or anti-rabbit IgG-HRP, which were visualized using an ECL detection kit (Thermo, A38555, SHH, CN).

The chemicals used in this study were GA, rapamycin, chloroquine, NMS873, and DBEQ. All buffers were prepared in deionized water and filtered through a 0.2-μm filter.

The primer sequences of the plasmid constructs are listed in Supplementary Table S1.

RESULTS

Gossypol acetate was identified as a VCP inhibitor that binds to the interface between the N and D1 domains

To identify novel modulators of VCP, we established a HTS biochemical assay for VCP ATPase activity measurement. We screened our in-house natural small-molecule library of 700 compounds (10 μM each; Supplementary Fig. S1a), and identified nine hits inhibiting VCP ATPase activity by ≥50%. The most potent compound was GA (Fig. 1a), an acetic acid mixture with gossypol that almost completely inhibited the ATPase activity of VCP at 10 μM (Supplementary Fig. S1a). Gossypol is an active component obtained from the seeds or root bark of *Malvaceae* or other plants. GA has better absorption, longer serum half-life, and fewer side effects than gossypol itself and has been widely used in the clinic [30]. We thus focused on GA for further study. GA inhibited VCP enzymatic activity at an IC_{50} of 6.53 ± 0.6 μM (Fig. 1b). To confirm the binding of GA to VCP, we performed a partial trypsin digestion assay using purified 6×His-VCP protein in the presence of gossypol, GA or the allosteric VCP inhibitor NMS873 [31] (Fig. 1c). We observed a significant difference in the cleavage profile between each inhibitor-treated group and the DMSO control group. GA and gossypol reduced VCP sensitivity to trypsin digestion compared to the effect of DMSO (Fig. 1c, red arrow), confirming their direct binding to VCP. Notably, the digestion patterns of the gossypol and GA groups were identical, as expected, and were quite different from that of NMS873, suggesting that the influence of NMS873 on VCP conformation is different from that of gossypol or GA. GA inhibited the ATPase enzymatic activity of both VCP-FL (full length) and the VCP-N + D1 domain but not that of the VCP-D1 + D2 domain (Fig. 1d), suggesting that inhibition of VCP enzymatic activity by GA required both the N and D1 domains of VCP.

To verify the binding of GA to VCP, we carried out a thermal shift assay based on the ligand-induced thermal stabilization of target proteins. The thermostability of the 6×His-VCP protein gradually increased with increasing concentrations of GA when the temperature was fixed at 70 °C (Supplementary Fig. S1b). VCP was significantly more stable in the 5 μM GA group than in the DMSO control group. Next, the VCP protein melting temperature (T_m) was determined upon its incubation with 5 μM GA or DMSO control. GA significantly increased the T_m of VCP, from 64.2 ± 0.1 °C to 71.1 ± 0.7 °C (Fig. 1e, f), confirming the direct binding of GA to VCP. Consistent with the result showing that VCP enzymatic inhibition by GA required the presence of both N and D1 domains, a thermal shift assay also confirmed that GA binds to the N + D1 domain. Incubation with 5 μM GA significantly increased the thermal stability of the VCP-N + D1 domain (the T_m increased from 56.9 ± 0.1 °C to 62.3 ± 1.6 °C (Fig. 1g, h). We then used ITC to quantify the interaction between VCP and GA. The calorimetry experiments showed that the K_D value was ~6.9 μM for the binding of GA and VCP (Supplementary Fig. S1c).

Next, we attempted to gain additional insight into the interaction by docking gossypol to the crystal structure of VCP (PDB ID 5DYG) in a simulation experiment. The result of the molecular docking experiment, which suggested that gossypol binds at the interface between the VCP N domain and D1 domain

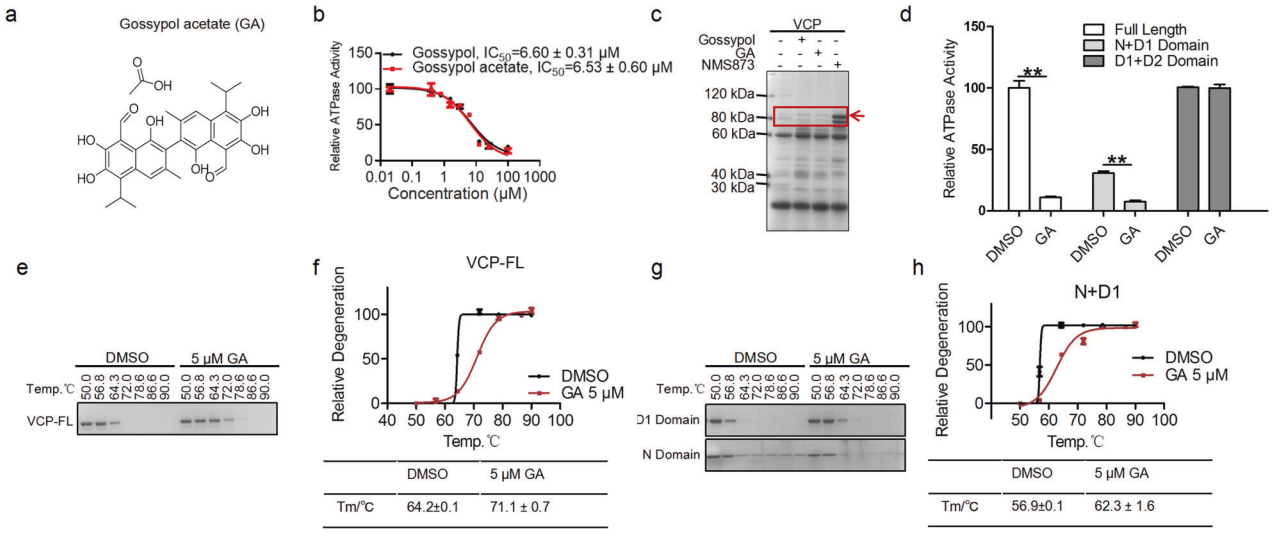

Fig. 1 Gossypol acetate bound to VCP and inhibited its ATPase activity in vitro. a 2D-chemical structure of gossypol acetate. **b** Dose-dependent curve of the inhibitory activity of gossypol acetate on VCP. The IC_{50} value for the inhibition of VCP ATPase activity was measured by the malachite green-based ATPase assay. The error bar represents the standard deviation (SD, $n = 3$). **c** Partial trypsin digestion analysis suggested direct binding of gossypol acetate to VCP. Purified 6×His-VCP protein was incubated with DMSO, gossypol, gossypol acetate, or NMS873 for 1 h at 37 °C in a total volume of 50 μL. After electrophoresis, the gels were stained with Coomassie brilliant blue. **d** Inhibition of ATPase activities of the VCP-FL, VCP-N + D1, or VCP-D1 + D2 domains by gossypol acetate was measured by the malachite green-based ATPase assay. The error (SD) based on three replicates is shown. $^{**}P < 0.01$. **e**, **f** Representative Coomassie brilliant blue and quantification data showing changes in the thermodynamic stability of purified 6×His-VCP in the presence of 5 μM gossypol acetate. The curves showing relative protein degradation are presented based on the mean and error (SEM) of three replicates. **g**, **h** Representative Coomassie brilliant blue and related quantification showing changes in the thermodynamic stabilities of purified 6×His-VCP-N and 6×His-VCP-N + D1 truncated proteins in the presence of 5 μM gossypol acetate. The curves of relative protein degradation are shown with the error (SD) of three replicates.

(Supplementary Fig. S1d), was consistent with the experimental results showing that the inhibition of VCP ATPase activity by GA required both the N and D1 domains. Given that the function of VCP relies on the formation of hexamers, we next used a native gel electrophoresis assay to determine whether GA affects VCP hexamer formation. The native gel electrophoresis of the product of VCP incubated with GA showed that the oligomeric state of the VCP complex was unchanged (Supplementary Fig. S1e). Together, these results demonstrated that GA is bound to the interface between the N and D1 domains of VCP, thereby inhibiting VCP ATPase activity in vitro without affecting its oligomeric state.

Gossypol acetate reduced the mHTT protein level and neuronal toxicity

As a crucial regulator of proteostasis, VCP regulates the degradation of damaged proteins in the proteasome and autophagy pathways. It has been implicated in the pathology of HD and other neurodegenerative diseases; thus, molecular modulators targeting VCP might be of therapeutic benefit for the treatment of neurodegenerative diseases, including Huntington's disease. We tested whether GA can facilitate the degradation of toxic, aggregation-prone mHTT and thus enhance neuron survival in HD cellular models.

We first investigated whether GA can promote the degradation of autophagy substrate-mHTT proteins in iPS-derived Q47 striatal neurons derived from HD patients as previously described [32]. The well-established HTRF assay was used for the measurement of mHTT levels [33] and assessment of mHTT clearance by GA treatment. The endogenous mHTT protein levels were decreased dose-dependently by GA treatment (Fig. 2a). The observed reduction was not due to cell loss because the total protein concentration for mHTT measurement was controlled. Moreover, compound treatment slightly increased the neuron cell number and improved cell morphology, as shown in Fig. 2d, excluding compound toxicity at the dose used. Western blot analysis was used to detect the levels of mHTT and wtHTT proteins. Antibodies against 2B7 and MW1 were used, with MW1 used to specifically detect polyQ mHTT and 2B7 used to detect both mHTT and wtHTT. As shown in Fig. 2b, GA induced an obvious reduction in mHTT and an increased ratio of LC3B-II versus LC3B-I, while the level of total HTT was only slightly decreased (Fig. 2b). Cotreatment with the autophagy inhibitor CQ almost completely blocked the degradation of mHTT and P62 and changed the trend of the LC3B-II to LC3B-I ratio induced by GA (Fig. 2c), implying that the observed mHTT reduction mainly depends on the autophagy pathway.

Since GA induced mHTT degradation, we next examined whether it can improve neuronal survival. Withdrawal of brain-derived neurotrophic factor (BDNF) induced neuronal apoptosis, cell shrinkage and loss, effects that were mHTT-dependent (Fig. 2d). These phenotypes under stress conditions were previously used for assaying Huntington's disease-associated cytotoxicity. Treatment with GA significantly reduced caspase-3 activation (Fig. 2d, e) and rescued stress-induced neuronal shrinkage and loss (Fig. 2d, f). The neuroprotective effect of GA was confirmed in the mouse striatal cell line $STHdh^{Q7/Q111}$ [34]. In this cell model, GA remarkably induced mHTT degradation in a dose-dependent manner, as shown by HTRF assay and Western blot analysis (Supplementary Fig. S2a, b). Consistently, GA reduced the apoptosis rate (determined by caspase-3 activation) induced by serum starvation (Supplementary Fig. S2c), indicating suppression of mHTT-induced cytotoxicity. To confirm the effect of GA on autophagy induction, we measured autophagic flux using HeLa cells stably expressing the tandem tagged fluorescent reporter mCherry-EGFP-LC3 to monitor the process of autophagosome maturation. In the neutral environment of the autophagosome, both green and red fluorescence are emitted. Once fused with lysosomes, autophagosomes become autolysosomes with increased acidity that quenches GFP. HeLa cells stably expressing mCherry-EGFP-LC3 were treated with GA, rapamycin and CQ to determine their effects on autophagic flux. As expected, autophagic flux was inhibited by CQ and activated by rapamycin

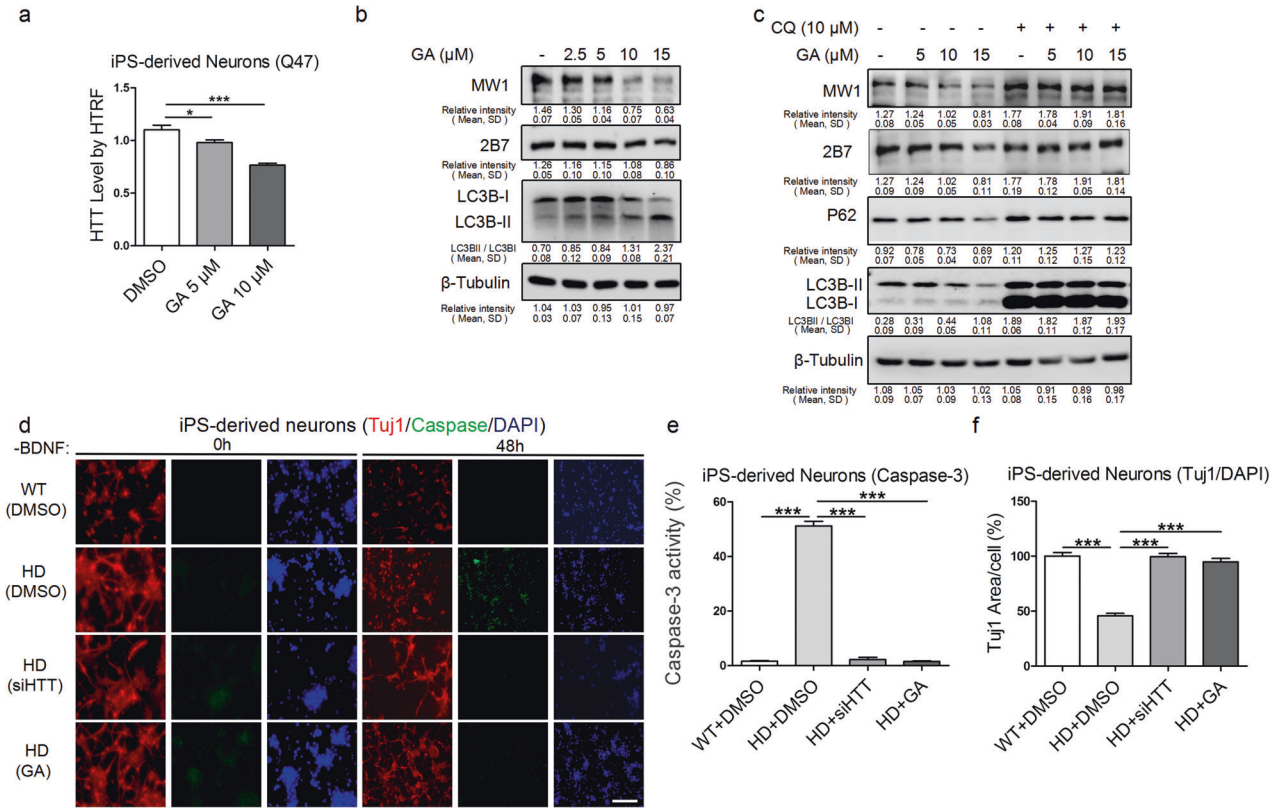

Fig. 2 Gossypol acetate reduced mHTT protein levels and neuronal toxicity in HD cell models. a Gossypol acetate treatment decreased mHTT levels in HD patient iPS-derived Q47 neuron cells, as shown by HTRF assay (2B7, MW1 for mHTT). HTRF quantification of the HTT levels in the Q47 cells treated with the indicated concentrations of gossypol acetate is shown. The data were normalized to the signal from the DMSO group. Statistical analyses were performed by one-way ANOVA, $^{*}P < 0.05$, $^{***}P < 0.001$, $n = 10$. **b** Representative Western blots showing the effect of gossypol acetate on mHTT levels. Q47 cells were treated with the indicated concentrations of gossypol acetate for 24 h. Cell lysates were immunoblotted with HTT antibodies (MW1 for mHTT or 2B7 for mHTT and wtHTT) and anti-LC3 antibodies. β-Tubulin was used during immunoblotting as a loading control. **c** Representative Western blots showing the gossypol acetate-induced blockade of the mHTT-lowering effect induced by the autophagy inhibitor CQ. Q47 cells were treated with gossypol acetate in the absence or presence of CQ for 24 h. Cell lysates were immunoblotted with anti-HTT antibodies (MW1 for mHTT or 2B7 for mHTT and wtHTT), anti-P62 antibodies and anti-LC3 antibodies. β-Tubulin was immunoblotted as a loading control. **d** Representative images of Tuj1 immunostaining and caspase-3 activity detection by a green florescent dye. Loss and shrinkage of HD patient iPS-derived neurons (Q47) under BDNF-deprived conditions, which was reversed by mHTT knockdown or gossypol acetate treatment, is shown (scale bar: 200 μm). **e** Quantification of caspase-3 activity in **d** corrected by cell number (by DAPI). The data were normalized to the DMSO control group (first bar). Statistical analyses were performed by one-way ANOVA with post hoc Dunnett's tests: $^{***}P < 0.001$. **f** Quantification of the Tuj1 signal in **d**. The covered area (Tuj1 area) was normalized by the nuclei counts. The Tuj1 area per cell reflects neuronal process shrinkage and loss. Data were normalized to the DMSO-treated control group (first bar). The statistical analysis was performed by one-way ANOVA with post hoc Dunnett's tests: $^{***}P < 0.001$. For all panels, the bars represent the mean and SD.

in the HeLa cells. GA resulted in a significantly increased ratio of red puncta versus green puncta, similar to those of rapamycin (Supplementary Fig. S2d and quantified in Supplementary Fig. S2e), indicating suppression of mHTT-induced cytotoxicity. In summary, GA treatment induced the degradation of mHTT proteins and significantly suppressed mHTT toxicity, which relies on autophagy.

Gossypol acetate increased the formation of the mHTT-VCP-LC3 ternary complex

We next investigated the mechanism by which GA induced mHTT degradation by harnessing autophagic machinery. Previous studies showed that VCP colocalized with expanded polyQ in HD mouse brains and in postmortem patient brains [14, 35]. We used a pull-down experiment to confirm the VCP-mHTT interaction and further revealed that the N-terminal domain of VCP is the binding site for mHTT (Supplementary Fig. S3a). In addition, it has been reported that VCP interacts with LC3 through the LIR motif in the N-terminal domain of VCP [26]. However, it remains unclear whether VCP forms in a complex with mHTT and LC3 or plays a role in autophagy-mediated mHTT degradation.

We carried out in vitro pull-down experiments to determine whether VCP formed a complex with mHTT or LC3 and examined the effects of GA on the VCP interaction with LC3 or mHTT. First, GA enhanced the interaction between GST-LC3 and 6×His-VCP in a dose-dependent manner (Fig. 3a). In contrast, the VCP enzymatic inhibitors NMS873 and DBEQ did not affect the interaction of VCP with LC3 (Supplementary Fig. S3b), in accordance with the observation that LC3 and mHTT have different binding sites on VCP and different trypsin digestion patterns. Second, we examined whether GA affected the interaction of VCP with mHTT or wtHTT. The pull-down assay revealed that the interaction of VCP with mHTT is much stronger than its interaction with wtHTT. GA significantly increased the binding strength of VCP with mHTT (Fig. 3b), but it had little influence on the VCP-wtHTT interaction. Next, we sought to determine whether VCP formed a complex with mHTT and LC3 and the effects of GA on the complex formation. Pull-down experiments showed that VCP formed a

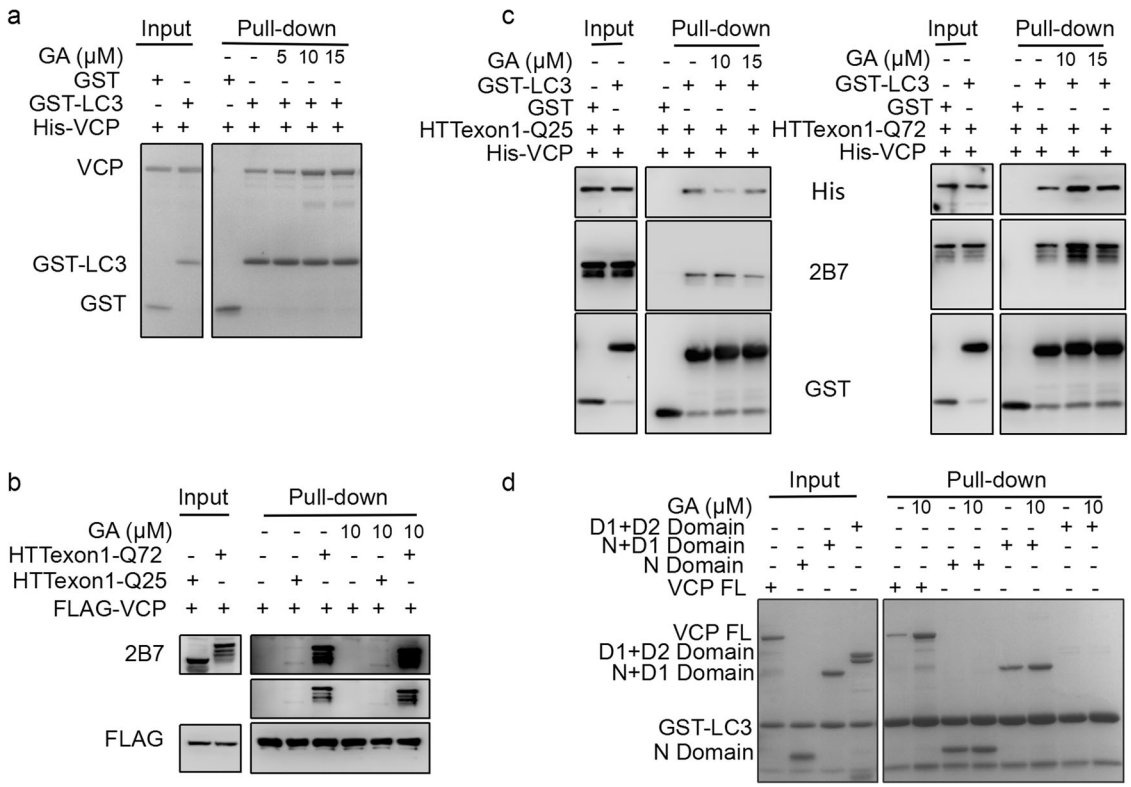

Fig. 3 Gossypol acetate enhanced LC3-VCP-mHTT ternary complex formation by targeting VCP. a In vitro pull-down assays using purified 6XHis-VCP protein incubated with GST-LC3 protein and gossypol acetate. Gossypol acetate or DMSO was added at the indicated concentrations for 1 h before pull-down using GST beads. Input and pull-down samples were stained by Coomassie brilliant blue (CBB). Gossypol acetate increased the interaction between VCP and LC3, as shown by Western blotting. **b** In vitro pull-down assays using purified Flag-VCP protein incubated with purified 6×His-mHTT-Q72 or 6×His-wtHTT-Q25 protein and gossypol acetate. Gossypol acetate or DMSO was added at the indicated concentrations for 1 h before pull down using anti-Flag beads. Input and pull-down samples were detected by Western blot with the indicated antibodies. Gossypol acetate increased the interaction between VCP and mHTT-Q72 but had little influence on the interaction of VCP with wtHTT-Q25 (2B7 for mHTT and wtHTT). **c** In vitro pull-down assays using purified 6×His-VCP protein, GST-LC3 protein, and the 6×His-mHTT-Q72 or 6×His-wtHTT-Q25 protein in the absence or presence of gossypol acetate. Gossypol acetate or DMSO was added at the indicated concentrations for 1 h before pull-down using GST beads. Input and pull-down samples were assessed by Western blotting with the indicated antibodies. Gossypol acetate enhanced the formation of the LC3-VCP-mHTT complex. **d** Enhanced LC3-VCP interaction by gossypol acetate depended on the presence of both the N and D1 domains. In vitro pull-down assays were performed using purified 6×His-VCP protein, the VCP N domain, and N + D1 or D1 + D2 truncated proteins. Gossypol acetate or DMSO was added at the indicated concentrations for 1 h before pull-down using anti-GST beads. Input and pull-down samples were detected by Coomassie brilliant blue (CBB).

complex with mHTT and LC3 (Fig. 3c). Consistent with the enhanced interaction of VCP-LC3 and VCP-mHTT, GA also increased the complex formation of 6XHis-VCP, GST-LC3, and mHTT proteins (Fig. 3c). However, in the absence of VCP, GA did not obviously affect the binding between GST-LC3 and mHTT-Q72 (Supplementary Fig. S3c), suggesting that enhanced LC3-VCP-mHTT complex formation depends on the effect of GA on VCP. VCP-FL, the VCP-N domain and the VCP-N + D1 domain interacted with LC3 (Fig. 3d), indicating that VCP interacts with LC3 through the N domain of VCP. GA increased the interaction of LC3 with VCP-FL and the VCP-N + D1 domain but not VCP-N alone. This finding suggests that the stronger VCP-LC3 interaction relies on GA binding to VCP, which depends on the presence of both the N and D1 domains (Fig. 1). These data revealed that GA enhanced the formation of the mHTT-VCP-LC3 complex, which may facilitate the autophagy-mediated degradation of mHTT by increasing the efficiency of substrate recognition by autophagosomes.

Gossypol acetate reduced mHTT levels and rescued HD-relevant phenotypes in vivo

Having demonstrated that GA protected HD neurons by inducing the autophagy-mediated degradation of mHTT, we assessed whether GA had a beneficial effect in vivo on *Drosophila* HD models expressing HTT-16Q, HTT-128Q, HTTexon1-25Q, or HTTexon1-72Q fragments [36]. As shown by HTRF assays, GA significantly reduced mHTT levels in the HTT-128Q model as well as in the HTTexon1-72Q model without reducing wtHTT levels in transgenic *Drosophila* models with HTT-16Q or HTTexon1-25Q (Fig. 4a). In the HTT-128Q flies, feeding food containing 10 μM GA significantly rescued the climbing deficits in Huntington's disease flies (Fig. 4b). The flies expressing HTTexon1-72Q exhibited similar climbing deficits and a shorter lifespan and were also rescued by food containing GA, while little effect after GA treatment was observed in the flies expressing wtHTT (HTT-16Q or HTTexon1-25Q; Figs. 4c, d). The results suggest that GA was effective in reducing the mHTT levels and reversing the HD phenotypes in the *Drosophila* models.

To confirm neuronal protective effects and therapeutic potential of GA, we examined the effects of GA in a HD knock-in mouse model expressing endogenous mHTT proteins with 140Q ($Hdh^{Q140/Q140}$). Consistent with previous reports, we observed several motor function-related deficits in homozygous HD ($HdhQ^{140/Q140}$) mice, including a decrease in activity in the rearing test, deficits in the open-field tests, and reduced latency to fall in the rotarod tests. Intraperitoneal injection of GA significantly rescued all these behavioral phenotypes (Fig. 5a–c). Consistently,

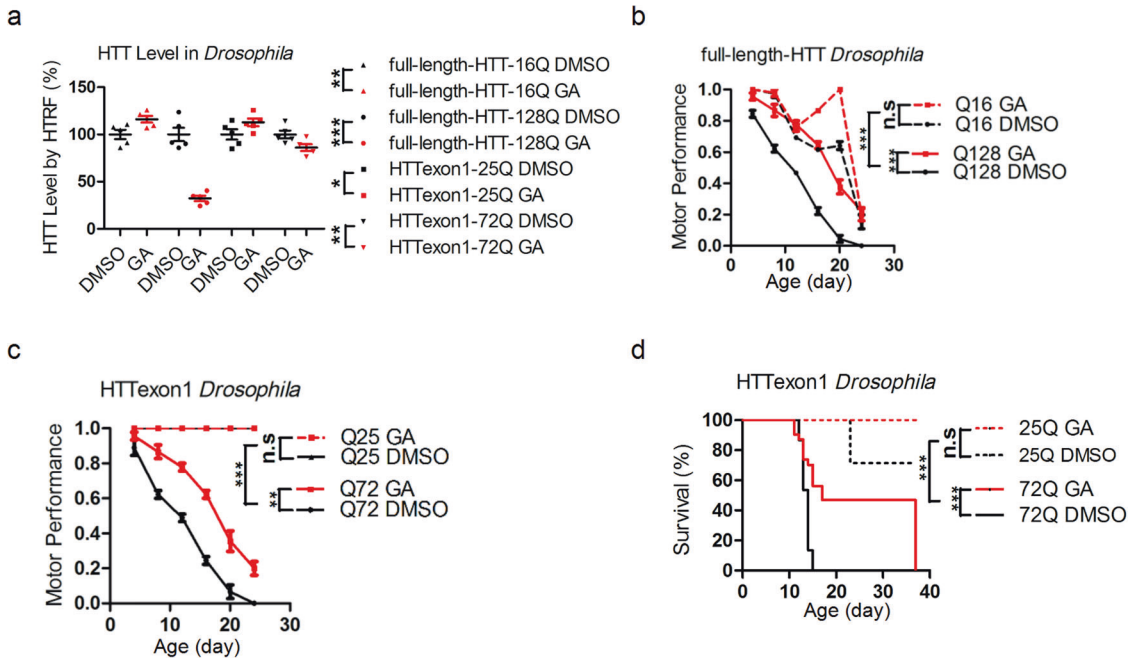

Fig. 4 Gossypol acetate reduced the mHTT levels and reversed the HD-relevant phenotypes in full-length HTT-128Q and HTTexon1-72Q transgenic flies. a Quantification of HTT levels in transgenic fly heads as indicated by HTRF measurements (using the 2B7 and MW1 antibody pairs). Transgenic *Drosophila* with *elav-GAL4*-driven expression of human full-length HTT-16Q (Full-Htt-16Q), Full-HTT-128Q (Full-Htt-128Q), HTTexon1-25Q (Exon1-HTT-25Q), or HTTexon1-72Q (Exon1-HTT-72Q) were fed with 10 μM gossypol acetate or DMSO for 2 weeks. Statistical analysis was performed by two-way ANOVA $^{*}P < 0.05$, $^{**}P < 0.01$ $^{***}P < 0.001$. **b** Gossypol acetate treatment reversed the motor behavior deficits in the transgenic mHTT *Drosophila* with the indicated genotypes. the Flies were fed 10 μM gossypol acetate or DMSO (black lines) for 2 weeks. The statistics were performed by two-way ANOVA. $^{***}P < 0.001$; ns no significance. **c** As in **b**, but using flies expressing HTT-exon 1 fragments with the indicated Q lengths. The statistics were performed by two-way ANOVA. $^{**}P < 0.01$, $^{***}P < 0.001$; ns, no significance. **d** Survival curves showing the transgene and compound treatment used. The flies were fed 10 μM gossypol acetate (red lines) or DMSO (black lines) for 2 weeks. The statistics were determined by log-rank test. $^{***}P < 0.001$; ns no significance. For all panels, the bars represent the mean and SD.

homozygous HD mice treated with GA showed significantly reduced mHTT levels in the cortex and striata (Fig. 5d). All the results confirmed that GA treatment reduced mHTT levels in vivo and reversed HD-relevant phenotypes.

DISCUSSION

VCP plays a critical role in governing proteostasis and protecting cells from cytotoxic effects caused by damaged proteins. Its dysfunction is related to the pathogenesis of neurodegenerative diseases; thus, VCP is believed to be a potential therapeutic target for the treatment of neurodegenerative disease. In the present study, we identified GA, a drug from traditional Chinese medicine for the treatment of uterine leiomyoma and endometriosis, as a novel inhibitor of the ATPase of VCP. We showed that GA induced the autophagy-mediated degradation of mHTT and reversed HD-relevant phenotypes.

We found that gossypol has a unique mechanism of action by enhancing the formation of the VCP-LC3-mHTT ternary complex, thus facilitating autophagy-mediated mHTT degradation. This unique mechanism distinguished it from previously reported VCP inhibitors and other autophagy inducers. Moreover, although VCP has been shown to colocalize with mHTT and is involved in HD pathogenesis [14], whether VCP plays a crucial role in autophagy-mediated mHTT degradation remains unclear. In our study, we revealed that the N-terminal domain of VCP mediated the formation of the VCP-LC3-mHTT ternary complex and facilitated the autophagy-mediated degradation of mHTT, which was significantly enhanced upon GA treatment. GA binding to VCP increased the interaction of VCP with LC3 and mHTT, thus leading to enhanced complex formation. In contrast, the formation of the wtHTT-VCP-LC3 complex was largely unaffected by GA treatment, and the interaction between VCP and wtHTT was much weaker than the interaction between VCP and mHTT, suggesting that gossypol selectively recruited mHTT to the ternary complex for autophagic degradation. Furthermore, the stronger interaction between mHTT and the LC3 complex requires VCP, as GA did not affect the binding of LC3 and mHTT in the absence of VCP. Considering these observations, we proposed a model in which GA binds to VCP acted in a gain-of-function manner to promote the formation of the mHTT-VCP-LC3 ternary complex, thus selectively accelerating autophagy-mediated degradation of mHTT. This mechanism of action of GA is completely different from previously reported VCP inhibitors and is similar to the mode of action of rapamycin and FK506, which act by inducing the formation of mTOR-rapamycin-FKBP12 and calcineurin-FK506-FKBP12 complexes, respectively [37, 38]. This action shows the unique value of small molecules, revealing a mechanism that cannot be captured by genetic deletion in knockdown experiments.

In contrast to previously reported VCP inhibitors that target the VCP D2 enzymatic domain, GA binds to the interface between the N and D2 domains and enhances VCP-N domain interactions with LC3 and mHTT. The N-terminal domain of VCP is involved in cofactor binding and substrate recognition [39, 40]. The interface between the N-domain and D1 domain was considered to be important for N-D1 communication, as well as D1-controlled conformational changes of the N domain, which in turn might regulate cofactor interactions. In our study, we demonstrated that the N-terminal domain is critical for the interaction of VCP with LC3 and with mHTT. GA binds to the interface between the N and D1 domains, and its inhibition of VCP enzymatic activity and its

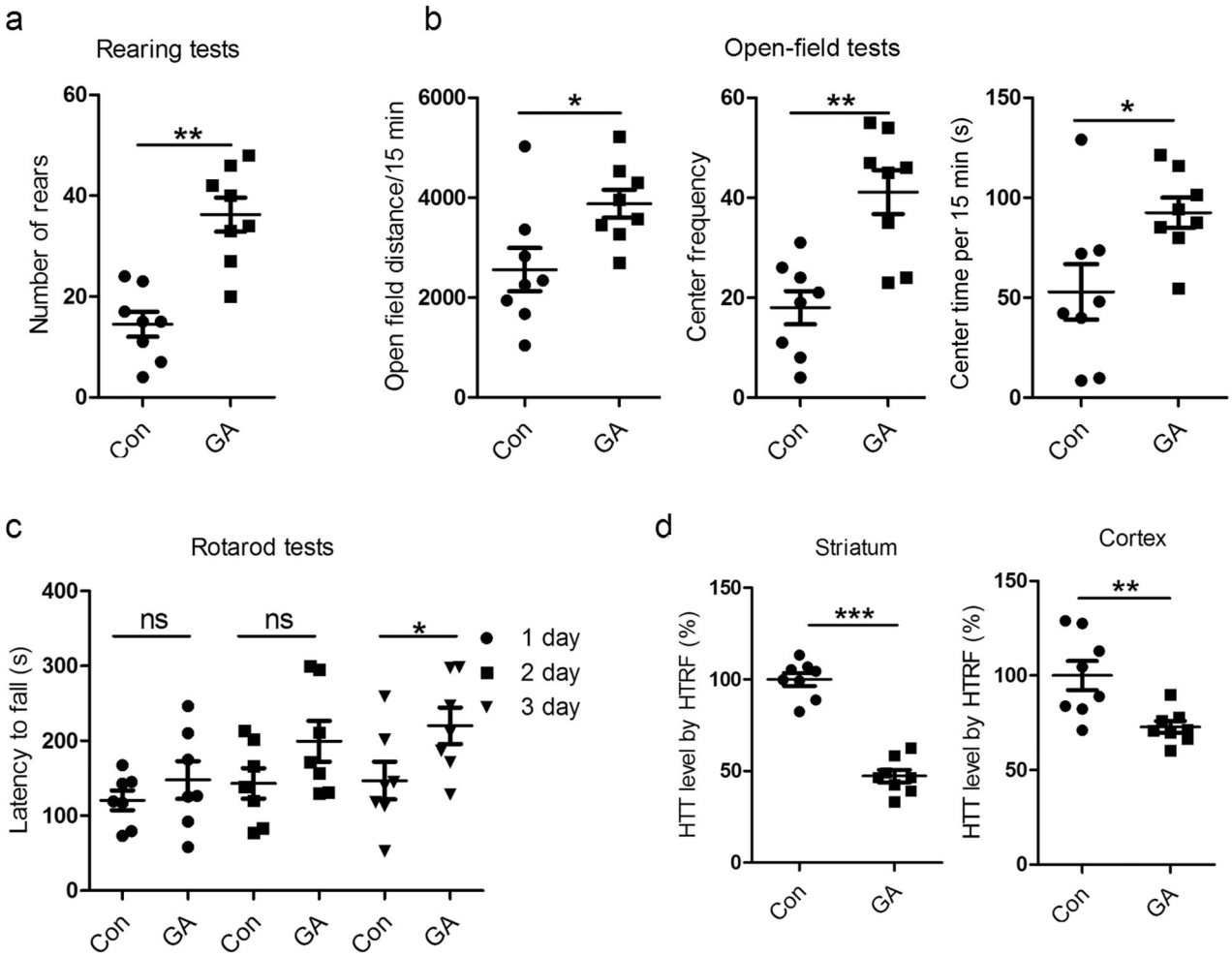

Fig. 5 Gossypol acetate reversed HD-relevant behavioral phenotypes in a knock-in Huntington's disease mouse model. a Rearing tests of 11-month-old Huntington's disease mice ($Hdh^{Q140/Q140}$) treated with gossypol acetate or vehicle. The mice were ip injected with 15 mg/kg gossypol acetate once every three days for 2 months. The number of rearing events per 5 min are shown. The statistical analysis was performed by two-tailed unpaired *t*-tests **, $P < 0.01$, $n = 8$. **b** Open-field tests of Huntington's disease mice ($Hdh^{Q140/Q140}$) after ip injection with gossypol acetate for 2 months. The statistical analysis was performed by two-tailed unpaired *t*-tests: *$P < 0.05$, **$P < 0.01$, $n = 8$. **c** Rotarod test results for the Huntington's disease mice ($Hdh^{Q140/Q140}$) after ip injection with gossypol acetate for 2 months. Each mouse was trained three times and then tested for 3 consecutive days. The statistical analyses were performed by two-tailed unpaired *t*-tests: *$P < 0.05$, $n = 8$. **d** Mutant HTT levels measured by HTRF in gossypol acetate- versus vehicle-treated mice. Mutant HTT levels were measured by HTRF. Both the striata and the cortices were tested. Eight mice in each group were measured. The statistical analysis was performed by two-tailed unpaired *t*-tests, **$P < 0.01$, ***$P < 0.001$, $n = 8$. For all panels, bars represent mean and SD.

interaction with VCP require the presence of both the N and D1 domains. The binding of GA to the VCP N-D1 interface strengthened the binding of VCP with both mHTT and LC3 without affecting VCP oligomerization. Thus, binding of GA to the N-D1 interface might regulate the N-terminal domain conformation and thus increase LC3-VCP-mHTT complex formation. Two other known inhibitors of VCP, NMS-873 and DBEQ, bind at different VCP positions, and our trypsin digestion pattern of VCP also indicated that the binding site of GA is quite different from that of NMS-873. As an interaction hub, VCP has multiple cofactor binding sites and diverse mechanisms to regulate distinct aspects of VCP-mediated processes. It has been reported that various disease-associated mutations might affect the association of VCP with certain cofactors, leading to the impairment of distinct subsets of VCP/p97 functions and different effects [10]. It is reasonable to think that inhibitors binding to different sites of VCP might regulate distinct functions of VCP [39].

We showed in this study that GA had beneficial effects in HD treatment by targeting VCP and harnessing autophagy machinery. Although gossypol has been used for the treatment of various diseases by targeting different proteins, this is the first time that its neuroprotective role has been identified and its unique underlying mechanism has been revealed. The improvement in neuronal survival induced by GA treatment was comparable to the effects of mHTT knockdown in human iPS-derived HD neurons. The neuronal protective effect of GA was potent and specific to mHTT-induced neuronal toxicity in vivo in *Drosophila* HD models. In our HD cell and mouse model, GA lowered the level of mHTT by ~20%–40% and reversed Huntington's disease-associated phenotypes. This outcome is reasonable since a previous study using a human ESC-derived neuronal model suggested that a 10%–20% reduction in mHTT alone is sufficient to show a significant reduction in toxicity, whereas reducing wtHTT by as much as ~90% seemed to render it safe [41]. Reducing mHTT protein has been proven to be an effective therapeutic approach in animal models and recent clinical trials [42]. Gossypol has been reported to penetrate the blood–brain barrier (BBB) [43]. In our study, GA improved HD-relevant motor function deficits in both *Drosophila* and mouse HD knock-in models. Thus, GA is a promising lead compound to use for developing new treatments for HD.

Binding of gossypol to VCP enhances mHTT-VCP-LC3 ternary complex formation and the ensuing degradation of the disease-causing mHTT protein. This novel mechanism of action, which bears similarity to rapamycin and FK506, represents a novel strategy in which small molecules are used to target VCP to facilitate the autophagy-mediated clearance of disease-causing mHTT. Recently, a tethering compound that interacts with both LC3 and mHTT was reported to target mHTT for autophagic degradation, reduce mHTT levels and reverse disease-relevant phenotypes [44]. Herein, gossypol acted similarly in a gain-of-function manner to induce mHTT degradation by autophagy; however, these effects depend on the regulation of VCP by gossypol. In summary, our study showed that small molecules targeting VCP have therapeutic potential for the treatment of HD, and we identified gossypol as the first small-molecule modulator of VCP in the selective autophagic degradation of mutant HTT. As gossypol has already been used as a drug in China for many years, our results also suggest that it can be directly repurposed for clinical evaluation as a new therapy for HD.

ACKNOWLEDGEMENTS

This work was supported by the National Natural Science Foundation of China (31270830 and 21572038 to YJD; 81870990 to BXL;81625022, 91853205, 81821005 to CL; 31970748 to YHF), the Science and Technology Commission of Shanghai Municipality (18431907100 and 19XD1404700 to C.L.), the Development Fund for Shanghai Talents, Fund of State Key Laboratory of Bioorganic and Natural Products Chemistry, and Fund of State Key Laboratory of Drug Research and Chinese Academy of Science (SIMM1601KF-08). The authors acknowledge instructive advice and support from Prof. Fang Huang from Fudan University and her student Yu-fang Yang, Prof. Jun O. Liu from the Johns Hopkins University and Prof. Jian-zhong Yu from the University of Kansas.

AUTHOR CONTRIBUTIONS

XJL performed the ATPase assay, PTS assay, pull-down assay, Western blot analysis, mouse behavioral experiments and the corresponding data analysis, and wrote the manuscript. YYZ contributed to manuscript writing and modification and was involved in the mouse behavioral experiments. YHF contributed to the HTRF assay, neuronal loss, and apoptosis measurement. HZ contributed to simulating the interaction model of GA and VCP. HXL completed *Drosophila* model behavior experiments. QFL was involved in performing the Western blot analysis. HLL was involved in the mouse behavioral experiments. RKT conducted the HTS. CXJ performed partial proteolysis assays and ITC experiments. WJ and ZXL were involved in protein expression and purification, ITC, and mouse behavioral experiments. CL conceived and supervised the simulation of the interaction model. BXL conceived and supervised the HD cell and animal experiments. YJD conceived and supervised the project and modified the manuscripts.

ADDITIONAL INFORMATION

The online version of this article (https://doi.org/10.1038/s41401-020-00605-0) contains supplementary material, which is available to authorized users.

Competing interests: The authors declare no competing interests.

REFERENCES

1. Rubinsztein DC. The roles of intracellular protein-degradation pathways in neurodegeneration. Nature. 2006;443:780–6.
2. Dürr A, Stevanin G, Cancel G, Duyckaerts C, Abbas N, Didierjean O, et al. Spinocerebellar ataxia 3 and machado-joseph disease: clinical, molecular, and neuropathoiogicai features. Ann Neurol. 1996;39:490–9.
3. Duyckaerts C, Delatour B, Potier MC. Classification and basic pathology of Alzheimer disease. Acta Neuropathol. 2009;118:5–36.
4. Iwai A, Masliah E, Yoshimoto M. The precursor protein of non-Ap component of Alzheimer's disease amyloid is a presynaptic protein of the central nervous system. Neuron. 1995;14:467–75.
5. Raymond LA, André VM, Cepeda C, Gladding CM, Milnerwood AJ, Levine MS. Pathophysiology of Huntington's disease: time-dependent alterations in synaptic and receptor function. Neuroscience. 2011;198:252–73.
6. Soto C. Unfolding the role of protein misfolding in neurodegenerative diseases. Nat Rev Neurosci. 2003;4:49–60.
7. Yu S, Liang Y, Palacino J, Difiglia M, Lu B. Drugging unconventional targets: insights from Huntington's disease. Trends Pharmacol Sci. 2014;35:53–62.
8. Tsvetkov AS, Arrasate M, Barmada S, Ando DM, Sharma P, Shaby BA, et al. Proteostasis of polyglutamine varies among neurons and predicts neurodegeneration. Nat Chem Biol. 2013;9:586–92.
9. A Kakizuka, VCP, a major ATPase in the cells, as a novel target for currently incurable disorders. Innovative Medicine: Basic Research and Development. Tokyo: Springer; (2015).
10. Meyer H, Weihl CC. The VCP/p97 system at a glance: connecting cellular function to disease pathogenesis. J Cell Sci. 2014;127:3877–83.
11. Bug M, Meyer H. Expanding into new markets-VCP/p97 in endocytosis and autophagy. J Struct Biol. 2012;179:78–82.
12. Tresse E, Salomons FA, Vesa J, Bott LC, Kimonis V, Yao TP, et al. VCP/p97 is essential for maturation of ubiquitin-containing autophagosomes and this function is impaired by mutations that cause IBMPFD. Autophagy. 2010;6:217–27.
13. Van den BJ, Meyer H. VCP/p97-mediated unfolding as a principle in protein homeostasis and signaling. Mol Cell. 2018;69:182–94.
14. Hirabayashi M, Inoue K, Tanaka K, Nakadate K, Ohsawa Y, Kamei Y, et al. VCP/p97 in abnormal protein aggregates, cytoplasmic vacuoles, and cell death, phenotypes relevant to neurodegeneration. Cell Death Differ. 2001;8:977–984.
15. Fujita K, et al. A functional deficiency of TERA/VCP/p97 contributes to impaired DNA damage repair in multiple polyglutamine diseases. Nat Commun. 2013;4:1816.
16. Yang H, Li JJ, Liu S, Zhao J, Jiang YJ, Song AX, et al. Aggregation of polyglutamine-expanded ataxin-3 sequesters its specific interacting partners into inclusions: implication in a loss-of-function pathology. Sci Rep. 2014;4:6410.
17. Levine B, Kroemer G. Biological functions of autophagy genes: a disease perspective. Cell. 2019;176:11–42.
18. Menzies FM, Fleming A, Caricasole A, Bento CF, Andrews SP, Ashkenazi A, et al. Autophagy and neurodegeneration: pathogenic mechanisms and therapeutic opportunities. Neuron. 2017;93:1015–34.
19. Sarkar S, Rubinsztein DC. Huntington's disease: degradation of mutant huntingtin by autophagy. FEBS J. 2008;275:4263–70.
20. Rubinsztein DC, Codogno P, Levine B. Autophagy modulation as a potential therapeutic target for diverse diseases. Nat Rev Drug Discov. 2012;11:709–30.
21. Jimenez-Sanchez M, Thomson F, Zavodszky E, Rubinsztein DC. Autophagy and polyglutamine diseases. Prog Neurobiol. 2012;97:67–82.
22. He H, Dang Y, Dai F, Guo Z, Wu J, She X, et al. Post-translational modifications of three members of the human MAP1LC3 family and detection of a novel type of modification for MAP1LC3B. J Biol Chem. 2003;278:29278–87.
23. Pankiv S, Clausen TH, Lamark T, Brech A, Bruun JA, Outzen H, et al. p62/SQSTM1 binds directly to Atg8/LC3 to facilitate degradation of ubiquitinated protein aggregates by autophagy. J Biol Chem. 2007;282:24131–45.
24. Wong E, Cuervo AM. Autophagy gone awry in neurodegenerative diseases. Nat Neurosci. 2010;13:805–11.
25. Bjørkøy G, Lamark T, Brech A, Outzen H, Perander M, Overvatn A, et al. p62/SQSTM1 forms protein aggregates degraded by autophagy and has a protective effect on huntingtin-induced cell death. J Cell Biol. 2005;171:603–14.
26. Guo X, Sun X, Hu D, Wang YJ, Fujioka H, Vyas R, et al. VCP recruitment to mitochondria causes mitophagy impairment and neurodegeneration in models of Huntington's disease. Nat Commun. 2016;7:12646.
27. Xie H, Yin J, Shah MH, Menefee ME, Bible KC, Reidy-Lagunes D, et al. A phase II study of the orally administered negative enantiomer of gossypol (AT-101), a BH3 mimetic, in patients with advanced adrenal cortical carcinoma. Invest New Drugs. 2019;37:755–62.
28. Magnaghi P, D'Alessio R, Valsasina B, Avanzi N, Rizzi S, Asa D, et al. Covalent and allosteric inhibitors of the ATPase VCP/p97 induce cancer cell death. Nat Chem Biol. 2013;9:548–56.
29. Y Yao, X Cui, I Al-Ramahi, X Sun, B Li, J Hou, et al. A striatal-enriched intronic GPCR modulates huntingtin levels and toxicity. Elife. 2015;4:e05449.
30. Baldo B, Paganetti P, Grueninger S. TR-FRET-based duplex immunoassay reveals an inverse correlation of soluble and aggregated mutant huntingtin in Huntington's Disease. Chem Biol. 2012;19:264–75.
31. Kwakye GF, Li D, Bowman AB. Novel high-throughput assay to assess cellular manganese levels in a striatal cell line model of Huntington's disease confirms a deficit in manganese accumulation. Neurotoxicology. 2011;3:630–9.
32. Almeida B, Abreu IA, Matos CA, Fraga JS, Fernandes S, Macedo MG, et al. SUMOylation of the brain-predominant Ataxin-3 isoform modulates its interaction with p97. Biochim Biophys Acta 2015;1852:1950–9.
33. Al-Ramahi I, Lam YC, Chen HK, de Gouyon B, Zhang M, Pérez AM, et al. CHIP protects from the neurotoxicity of expanded and wild-type Ataxin-1 and promotes their ubiquitination and degradation. J Biol Chem. 2006;281:26714–24.

34. Liu J, Farmer JD Jr, Lane WS, Friedman J, Weissman I, Schreiber SL. Calcineurin is a common target of cyclophilin-cyclosporin A and FKBP-FK506 complexes. Cell. 1991;66:807–15.
35. Huai Q, Kim HY, Liu Y, Zhao Y, Mondragon A, Liu JO, et al. Crystal structure of calcineurin-cyclophilin-cyclosporin shows common but distinct recognition of immunophilin-drug complexes. Proc Natl Acad Sci USA. 2002;99:12037–42.
36. Chapman E, Maksim N, de la Cruz F, La JJ. Clai, inhibitors of the AAA+ chaperon p97. Molecules. 2015;20:3027–49.
37. Meyer H, Bug M, Bremer S. Emerging functions of the VCP/p97 AAA-ATPase in the ubiquitin system. Nat Cell Biol. 2012;1:117–23.
38. Lu B, Palacino J. A novel human embryonic stem cell-derived Huntington's disease neuronal model exhibits mutant huntingtin (mHTT) aggregates and soluble mHTT-dependent neurodegeneration. FASEB J. 2013;27:1820–9.
39. Tabrizi SJ, Leavitt BR, Landwehrmeyer GB, Wild EJ, Saft C, Barker RA, et al. Targeting huntingtin expression in patients with Huntington's disease. N Engl J Med. 2019;380:2307–16.
40. Park J, Shim JK, Kang JH, Choi J, Chang JH, Kim SY, et al. Regulation of bioenergetics through dual inhibition of aldehyde dehydrogenase and mitochondrial complex I suppresses glioblastoma tumorspheres. Neuro Oncol. 2018;20:954–65.
41. Li J, Wang C, Wang Z, Zhu C, Li J, Sha T, et al. Allele-selective lowering of mutant HTT protein by HTT-LC3 linker compounds. Nature. 2019;575:203–9.
42. Chang L, Bertelsen EB, Wisén S, Larsen EM, Zuiderweg ER, Gestwicki JE. High-throughput screen for small molecules that modulate the ATPase activity of the molecular chaperone DnaK. Anal Biochem. 2008;372:167–76.
43. Weiss A, Abramowski D, Bibel M, Bodner R, Chopra V, DiFiglia M, et al. Single-step detection of mutant huntingtin in animal and human tissues:A bioassay for Huntington's disease. Anal Biochem. 2009;395:8–15.
44. Hickey MA, Zhu C, Medvedeva V, Lerner RP, Patassini S, Franich NR, et al. Improvement of neuropathology and transcriptional deficits in CAG 140 knock-in mice supports a beneficial effect of dietary curcumin in Huntington's disease. Mol Neurodegener. 2012;7:12.